



OPEN

Carbon dioxide inhibits UVB-induced inflammatory response by activating the proton-sensing receptor, GPR65, in human keratinocytes

Keimon Sayama^{1,2}, Katsuyuki Yuki¹, Keiichi Sugata¹, Satoko Fukagawa¹, Tetsuji Yamamoto¹, Shigaku Ikeda² & Takatoshi Murase¹✉

Carbon dioxide (CO₂) is the predominant gas molecule emitted during aerobic respiration. Although CO₂ can improve blood circulation in the skin via its vasodilatory effects, its effects on skin inflammation remain unclear. The present study aimed to examine the anti-inflammatory effects of CO₂ in human keratinocytes and skin. Keratinocytes were cultured under 15% CO₂, irradiated with ultraviolet B (UVB), and their inflammatory cytokine production was analyzed. Using multiphoton laser microscopy, the effect of CO₂ on pH was observed by loading a three-dimensional (3D)-cultured epidermis with a high-CO₂ concentration formulation. Finally, the effect of CO₂ on UVB-induced erythema was confirmed. CO₂ suppressed the UVB-induced production of tumor necrosis factor- α (TNF α) and interleukin-6 (IL-6) in keratinocytes and the 3D epidermis. Correcting medium acidification with NaOH inhibited the CO₂-induced suppression of TNF α and IL-6 expression in keratinocytes. Moreover, the knockdown of H⁺-sensing G protein-coupled receptor 65 inhibited the CO₂-induced suppression of inflammatory cytokine expression and NF- κ B activation and reduced CO₂-induced cyclic adenosine monophosphate production. Furthermore, the high-CO₂ concentration formulation suppressed UVB-induced erythema in human skin. Hence, CO₂ suppresses skin inflammation and can be employed as a potential therapeutic agent in restoring skin immune homeostasis.

The skin is the largest organ of the human body. It acts as a protective covering while serving as a barrier separating the body from the external environment. The stratum corneum and tight junctions in the granular layers prevent the entry of external stimuli such as antigens, microorganisms, and ultraviolet (UV) radiation from the external environment, as well as water evaporation from the internal environment¹. When antigens and pathogens enter the skin through these physical barriers, resident/infiltrated immune cells induce an immune response to eliminate them. Epidermal keratinocytes, which are responsible for building a physical barrier, play an important role in skin immunity and cooperate with immune cells by producing various growth factors, cytokines, and chemokines in response to external stimuli². In addition, UV radiation from sunlight is a major stress source for keratinocytes and affects various biological functions including the nervous system and endocrine system through the skin³. UV-induced oxidative stress leads to mitochondrial dysfunction and activation of the nuclear factor kappa B (NF- κ B) pathway, a major inflammatory response pathway, resulting in cell death^{4–6}. On the other hand, there are multiple UV-responsive stress proteins in keratinocytes, such as the NF-E2 related factor (NRF) family, which play a role in suppressing oxidative stress to prevent excessive cell death^{7–9}. Consequently, the skin functions as an immunological organ; however, excessive immune responses can lead to chronic skin inflammation and further to inflammatory skin diseases such as atopic dermatitis and psoriasis¹⁰. These diseases are difficult to cure and are accompanied by physical and mental stress due to skin symptoms that significantly reduce the quality of life, such as pruritus, redness, and lichenification. Therefore, the daily prevention of excessive immune responses is vital for maintaining skin immune homeostasis.

¹Biological Science Research, Kao Corporation, 2606, Akabane, Ichikai-machi, Haga-gun, Tochigi 321-3497, Japan. ²Department of Dermatology and Allergology, Juntendo University Graduate School of Medicine, Tokyo, Japan. ✉email: murase.takatoshi@kao.com

Carbon dioxide (CO₂) is one of the principal gas molecules responsible for aerobic respiration. In the cell, CO₂, a by-product of oxidative metabolism in the tricarboxylic acid (TCA) cycle, passively diffuses through the body and is expelled via the lungs by red blood cells. In mammals, neurons in the brainstem and the peripheral carotid body detect blood CO₂ pressure, usually maintained at approximately 40 mmHg¹¹. This CO₂-sensing system also exists in flies and nematodes^{12,13}, implying that CO₂ homeostasis is critical for the survival of various species.

Some gas molecules have been shown to function as signaling mediators called ‘gasotransmitters’¹⁴. Among them, hydrogen sulfide and nitric monoxide are well-known and are involved in physiological functions in the skin, such as vasodilation, cell proliferation, apoptosis, and inflammation^{15,16}. These facts suggest that gasotransmitters play an important role in maintaining skin homeostasis. Recent studies have reported that CO₂ improves alveolar damage in rat models and patients with acute respiratory distress syndrome^{17–19}. In addition, CO₂ has been shown to suppress lipopolysaccharide (LPS)-induced inflammatory responses in several blood cell types and lung-derived cell lines^{20–22}. Consequently, this points to CO₂ not only as a by-product of aerobic respiration but also to its role as a gasotransmitter in suppressing inflammatory responses. In the skin, CO₂ has been shown to improve wound healing and seasonal barrier dysfunction^{23–25}; inflammation is known to be strongly involved in skin wound healing and barrier functions as well as the circulatory system. The wound-healing process consists of three phases: the inflammatory phase, proliferative phase, and stable phase; this process may be delayed when an excessive inflammatory response is triggered during the inflammatory phase²⁶. Various cytokines secreted from keratinocytes, fibroblasts, and inflammatory cells are critical factors that influence skin barrier function and keratinocyte differentiation²⁷; however, little is known about the relationship between CO₂ and skin inflammation.

In the present study, the anti-inflammatory mechanism of CO₂ was elucidated using a UVB-irradiated human keratinocyte model, focusing on the CO₂-induced decrease in extracellular pH. In addition, the effect of CO₂ on UV-induced erythema was evaluated in human skin.

Results

CO₂ inhibited UVB-induced cytokine expression in HEK_n and the 3D epidermis. Human epidermal keratinocytes isolated from neonatal foreskin (HEK_n) cultured in 15% CO₂ displayed a significantly lower UVB-induced increase in TNF α and IL-6 mRNA expression (Fig. 1a,b) alongside significantly lower TNF α and IL-6 protein levels in the culture supernatant (Fig. 1c,d). In addition, the 3D epidermis treated with the high-CO₂ concentration formulation (CO₂) displayed a significantly lower UVB-induced increase in TNF α and IL-6 mRNA expression than the 3D epidermis treated with the control (Ctl) formulation (Fig. 1e,f). Taken together, these data indicate that CO₂ suppresses the production of UVB-induced inflammatory cytokines in the epidermis.

CO₂ induced extracellular acidification, which produced anti-inflammatory effects. pH changes in the 3D epidermis were visualized using the pH-dependent fluorescent indicators, BCECF and BCECF-AM. BCECF can selectively visualize extracellular pH due to its membrane impermeability, whereas BCECF-AM can selectively visualize intracellular pH as it is hydrolyzed into membrane-impermeable BCECF by cytosolic esterase. In this study, we found that extracellular BCECF-derived fluorescence was attenuated when the high-CO₂ concentration formulation was applied to the surface of the 3D epidermis (Fig. 2a) and the extracellular BCECF-derived representative FT decreased significantly, suggesting that CO₂ administration caused extracellular acidification (Fig. 2b). In the HEK_n, UVB-induced increases in TNF α and IL-6 mRNA expression were significantly suppressed depending on the acidification of the culture medium (Fig. 2c,d). Moreover, when the pH of the culture medium was neutralized using NaOH under 15% CO₂ condition, the CO₂-induced suppression of TNF α and IL-6 mRNA expression was reduced (Fig. 2e,f). Thus, these results indicate that CO₂-induced extracellular acidification may suppress UVB-induced inflammatory cytokine expression.

CO₂-activated GPR65 signaling suppressed UVB-induced inflammation by inhibiting NF- κ B activation in HEK_n. Extracellular pH changes are detected by H⁺-sensing GPCRs²⁸. It was determined that GPR65 mRNA was highly expressed in HEK_n compared to other H⁺-sensing GPCRs (Fig. 3a). Therefore, GPR65 was knocked down in HEK_n using GPR65-specific siRNA to clarify its role in CO₂-induced anti-inflammatory effects (Fig. 3b). GPR65 knockdown significantly inhibited the CO₂-induced downregulation of TNF α and IL-6 mRNA expression (Fig. 3c,d); furthermore, it diminished the CO₂-induced suppression of inhibitor- κ B α (I- κ B α) degradation and p65 nuclear translocation caused by UVB irradiation (Fig. 3e,f). However, no difference was observed in the UVB-induced phosphorylation of p38, extracellular signal-regulated 1/2 (ERK1/2), or c-Jun N-terminal kinase (JNK) following 15% CO₂ incubation or GPR65 knockdown (Fig. 3g). Culture under 15% CO₂ significantly increased the intracellular cAMP concentration; however, this CO₂-induced increase was diminished by GPR65 knockdown (Fig. 3h). Moreover, when dibutyryl cAMP, a cAMP analog, was added to clarify the anti-inflammatory effect of cAMP in HEK_n, UVB-induced TNF α and IL-6 mRNA expressions were significantly suppressed in a concentration-dependent manner (Fig. 3i,j). Taken together, these results indicate that CO₂-induced extracellular acidification activates GPR65, increases intracellular cAMP concentration, and inhibits UVB-induced NF- κ B activation.

CO₂ inhibited UVB-induced erythema in human skin. To clarify the anti-inflammatory effects of CO₂ on human skin, control and high-CO₂ concentration formulations were applied to the skin on the inner upper arm of nine men, followed by UVB irradiation. UVB-induced skin erythema formation and MED were suppressed in the skin area where CO₂ had been applied (Fig. 4a,b). In addition, the Δa^* value (obtained by sub-

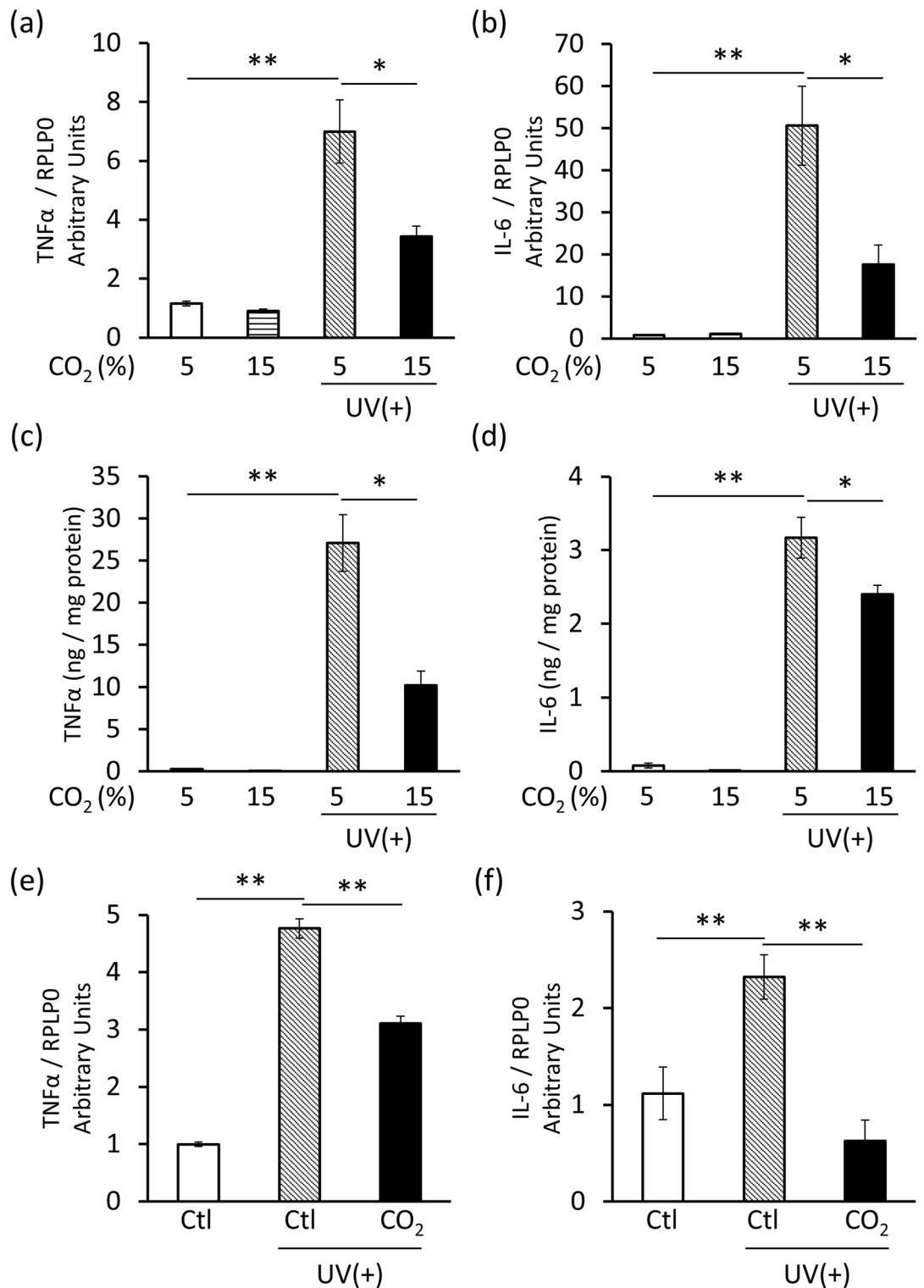


Figure 1. CO₂ inhibits UVB-induced cytokine expression in HEK293T and the 3D epidermis. **(a,b)** HEK293T cells were incubated in 5 or 15% CO₂ for 24 h and then irradiated with 20 mJ/cm² of UVB. Total RNA was isolated 8 h later and qRT-PCR was performed to detect TNFα and IL-6 mRNA expression ($n=3$, * $P<0.05$, ** $P<0.01$ vs. 5% CO₂ UV(+), Dunnett's test). **(c,d)** The culture supernatant was collected 24 h after UVB irradiation and ELISA was performed to measure TNFα and IL-6 concentration ($n=3$, * $P<0.05$, ** $P<0.01$ vs. 5% CO₂ UV(+), Dunnett's test). **(e,f)** CO₂-free (Ctl) and high-CO₂ concentration (CO₂) formulations were applied to the surface of the 3D epidermis for 12 h and then exposed to UVB. Total RNA was isolated 8 h later, and qRT-PCR was performed to detect TNFα and IL-6 mRNA expression ($n=3$, ** $P<0.01$ vs. Ctl UV(+), Dunnett's test).

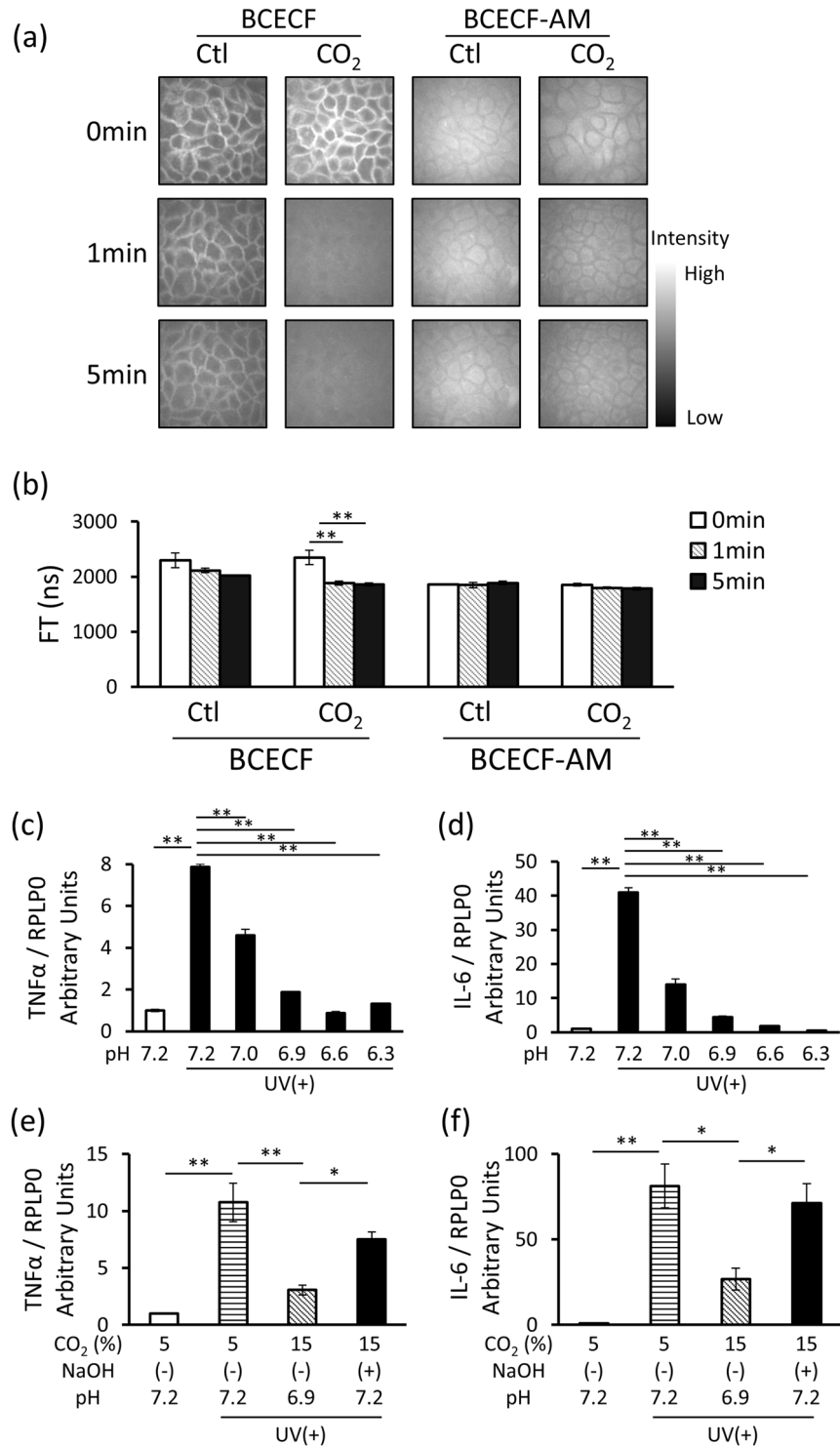


Figure 2. CO₂ induces extracellular acidification, generating anti-inflammatory effects. **(a)** CO₂-free (Ctl) and high-CO₂ concentration (CO₂) formulations were applied to the surface of the 3D epidermis after exposure to BCECF or BCECF-AM. Intra-epidermal pH was visualized by multiphoton laser microscopy (DermaInspect). Fluorescent images were obtained 0, 1, and 5 min after formulation application. The images shown are representative of three experiments with similar results. **(b)** Representative fluorescence lifetime was calculated from the fluorescent images using SPC Image 2.9.4 ($n = 3$, $**P < 0.01$ vs. CO₂ 0 min, Dunnett's test). **(c,d)** HEK293T cells were maintained at the indicated pH in an HCl-supplemented medium for 24 h and then irradiated with 20 mJ/cm² of UVB. Total RNA was isolated 8 h later, and qRT-PCR was performed to detect TNFα and IL-6 mRNA expression ($n = 3$, $**P < 0.01$ vs. pH 7.2 UV(+), Dunnett's test). **(e,f)** HEK293T cells were incubated in 5 or 15% CO₂ for 24 h and then irradiated with 20 mJ/cm² of UVB. The low pH (6.9) induced by 15% CO₂ was adjusted to pH 7.2 with NaOH. Total RNA was isolated 8 h later and qRT-PCR was performed to detect TNFα and IL-6 mRNA expression ($n = 3$, $*P < 0.05$, $**P < 0.01$, Tukey–Kramer test).

tracting the a^* value of the non-irradiated site from that of the site irradiated with 1MED UVB) was significantly lower in the skin area where CO₂ had been applied (Fig. 4c). Thus, these results indicate that CO₂ may exert anti-inflammatory effects in human skin.

Discussion

UV radiation emitted from the sun induces skin inflammation, which causes a wide range of skin symptoms from spots and wrinkles to dermatitis and skin cancer. In the present study, the anti-inflammatory effects of CO₂ were examined using a UVB-induced inflammation model. It was found that CO₂ suppressed TNF α and IL-6 production in human keratinocytes and the 3D epidermis and attenuated UVB-induced erythema formation in human skin. Since inflammatory cytokines such as TNF α and IL-6 are known to play key roles in skin inflammation^{29,30}, CO₂ may reduce UV-induced inflammation by suppressing their production.

The percutaneous administration of CO₂ has been shown to increase blood flow in the skin by reducing vascular smooth muscle tension under the epidermis^{31,32}, signifying that CO₂ has relatively high transdermal permeability. Therefore, CO₂ may permeate through the stratum corneum and react with H₂O in the interstitial fluid to produce H⁺, resulting in mild extracellular acidification. Consequently, the role of extracellular pH in the anti-inflammatory effects of CO₂ was investigated. In keratinocytes, the CO₂-induced suppression of TNF α and IL-6 expression was dependent on the pH of the culture medium, indicating that extracellular pH exerts important effects on skin inflammation. Interestingly, it has been reported that UV irradiation induces intracellular pH reduction and cell death in keratinocytes³³. These findings suggest that intracellular and extracellular pH changes exert different physiological effects. In the skin, the pH of the stratum corneum is known to play an important role in various pathological conditions. It is usually maintained in an acidic range of 4.1–5.8; however, it registers an increase in inflammatory skin diseases³⁴. Previous studies have shown that the disturbance of pH homeostasis disrupts various skin functions such as the antimicrobial response, skin barrier action, and inflammation^{35–37}. Thus, the topical application of CO₂ may improve the barrier and antimicrobial functions of the stratum corneum and suppress excessive inflammatory responses in the epidermis via CO₂-induced acidification.

Cells detect extracellular pH via acid-sensing ion channels and H⁺-sensing GPCRs^{28,38}. Although Na⁺/H⁺ exchanger 1 (NHE1) has been reported to sense extracellular pH changes in the skin^{39,40}, the biological sensors linking pH changes to skin inflammatory responses have not yet been elucidated. In the present study, it was demonstrated for the first time that GPR65, an H⁺-sensing GPCR, may detect CO₂-induced extracellular acidification and exert anti-inflammatory effects in keratinocytes. GPR65 has been reported to act as a psychosine receptor⁴¹; however, it has also been found to act as an H⁺ sensor^{42–44}, whose activation induces cAMP production via G α_s signaling. In the present study, GPR65 knockdown in keratinocytes suppressed CO₂-induced cAMP production, while dibutyl cAMP, a cAMP analog, inhibited TNF α and IL-6 expressions. These results indicate that CO₂-induced GPR65/cAMP signaling plays an important role in suppressing inflammation. There are various types of G α subunits (G α_s , G α_i , G α_q , and G α_{12}), each transmitting different cellular signals⁴⁵; however, it remains unclear whether GPR65 activates other G α proteins.

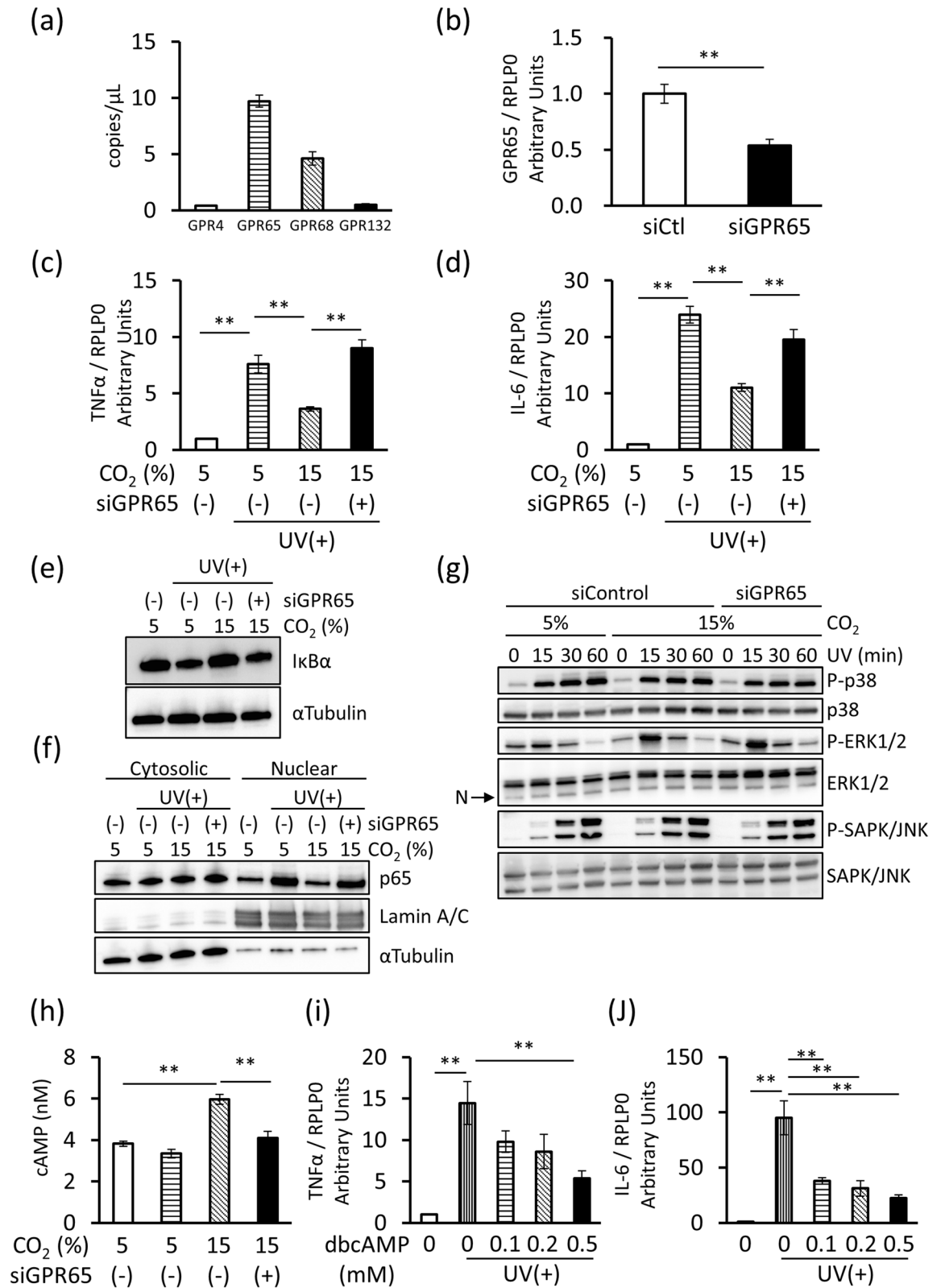
UV irradiation is known to induce inflammatory responses by MAPK and NF- κ B⁴⁶. In this study, CO₂ did not affect the phosphorylation of p38, ERK1/2, or JNK, implying that CO₂ does not exert its anti-inflammatory effects via the MAPK pathway. However, CO₂ did suppress UVB-induced I- κ Ba degradation and p65 nuclear translocation, while GPR65 knockdown opposed the CO₂-induced suppression of NF- κ B activation. Based on these results, it was hypothesized that CO₂ exerts its anti-inflammatory effects by activating GPR65 and following suppression of the NF- κ B pathway. While this finding is partly consistent with a previous work by Cummins et al.⁴⁷, other studies have shown that CO₂ does not affect I- κ Ba degradation in LPS-sensitized THP-1 cells and macrophages²². These conflicting results may be due to different NF- κ B activation mechanisms since it was recently reported that there is a third UV-dependent NF- κ B activation pathway in addition to the canonical and non-canonical pathways⁴⁸. In this pathway, I- κ Ba is translocated into the nucleus by UV irradiation without phosphorylation, where it is degraded by forming a complex with β -Transducin repeat Containing Protein (β -TrCP), a subunit of the ubiquitin-protein ligase complex, using IKK β as a scaffold. Therefore, GPR65 activation may affect this UV-dependent NF- κ B pathway; however, further studies are required to elucidate the detailed mechanism.

Skin inflammation is strongly involved in the pathogenesis of inflammatory skin diseases⁴⁹. Indeed, previous studies have shown that the inhibition of phosphodiesterase 4 (PDE4), a cAMP-degrading enzyme, improves atopic dermatitis and psoriasis^{50,51}; consequently, certain PDE4 inhibitors have been approved to treat these diseases^{52,53}. These clinical results suggest that cAMP plays a key role in the pathogenesis of inflammatory skin diseases. Since CO₂ has been shown to promote cAMP production in keratinocytes, it may exert a similar, albeit mild, effect as PDE4 inhibitors. Thus, the topical application of CO₂ may serve as a novel therapeutic approach for treating patients with inflammatory skin disorders.

In conclusion, in the present study, it was demonstrated that CO₂ activates GPR65 via extracellular acidification and exerts anti-inflammatory effects by suppressing NF- κ B activation in keratinocytes. Moreover, the topical application of a high-CO₂ concentration formulation inhibited UVB-induced erythema formation, implying that CO₂ suppresses skin inflammation in vivo. Therefore, our hypothesis, derived from the obtained results, states that CO₂ is a unique gas molecule that can suppress skin inflammation.

Methods

High-CO₂ concentration formulation. The formulations used in the present study were prepared as described previously²⁵. The high-CO₂ concentration and control formulations used the same base composition; however, the high-CO₂ concentration formulation contained ~1500–2000 ppm of CO₂ in the form of microbubbles.



◀ **Figure 3.** CO₂-activated GPR65 signaling suppresses UVB-induced inflammation by inhibiting NF-κB activation in HEK293T. **(a)** Digital PCR was performed to determine the mRNA expression of proton sensing GPCRs in HEK293T ($n=3$). **(b)** The cells were transfected with control non-target siRNA (siCtrl) or specific siRNA against GPR65 (siGPR65). Total RNA was isolated 48 h later and qRT-PCR was performed to detect GPR65 mRNA expression ($n=3$, $**P<0.01$, unpaired Student's *t* test). **(c,d)** The transfected cells were incubated in 5 or 15% CO₂ for 24 h and then irradiated with 20 mJ/cm² of UVB. Total RNA was isolated after 8 h, and qRT-PCR was performed to detect TNFα and IL-6 mRNA expression ($n=3$, $**P<0.01$, Tukey–Kramer test). **(e)** The cells were transiently transfected with siCtrl or siGPR65, incubated in 5 or 15% CO₂ for 24 h, and irradiated with 20 mJ/cm² of UVB. Whole cell extracts were prepared 8 h later, and I-κBα and α-tubulin levels were assessed by western blot analysis. **(f)** Cytoplasmic and nuclear extracts were prepared 8 h after UVB irradiation, and p65, laminin A/C, and α-tubulin levels were assessed by western blot analysis. **(g)** Whole cell extracts were prepared 0, 15, 30, and 60 min after UVB irradiation and P-p38, p38, P-Erk1/2, Erk1/2, P-SAPK/JNK, and SAPK/JNK levels were assessed by western blot analysis. ‘N’ on the left indicates a non-specific band. Luminescent signal images are shown cropped and full-length blots/gels are presented in Supplementary Figures 1–6. **(h)** The cells were transiently transfected with siCtrl or siGPR65. After 48 h, the cells were cultured in 5 or 15% CO₂ for 24 h with 0.5 mM IBMX, and then intracellular cAMP was measured ($n=3$, $**P<0.01$ vs. CO₂ 15% siGPR65(-), Dunnett's test). **(i,j)** The cells were incubated with 0, 0.1, 0.2, or 0.5 mM of dibutyryl cAMP (dbcAMP) for 24 h and then irradiated with 20 mJ/cm² of UVB. Total RNA was isolated 8 h later, and qRT-PCR was performed to detect TNFα and IL-6 mRNA expression ($n=3$, $**P<0.01$ vs. dbcAMP 0 mM UV(+), Dunnett's test).

Cell cultures. HEK293T (Invitrogen, Carlsbad, CA, USA) isolated from the foreskin of neonatal Caucasian subjects was cultured in EpiLife medium (Gibco, Waltham, MA, USA) supplemented with additive agents (HuMedia-KG kit; KURABO, Osaka, Japan). Before the experiments, the culture medium was replaced with fresh medium without additive agents. For the high-CO₂ experiments, cells were cultured in a humidified incubator under 15% CO₂ for 24 h. For the low-pH experiments, cells were cultured in a pH-modified culture medium for 24 h, with 1 M HCl and 1 M NaOH used to adjust the pH of the culture medium. For dibutyryl cAMP (dbcAMP; Sigma-Aldrich, St. Louis, MO, USA) treatment, cells were incubated with 0.1, 0.2, and 0.5 mM of dbcAMP for 24 h.

A three-dimensional (3D) epidermis (LabCyte EPI-MODEL 12; Japan Tissue Engineering Co. Ltd, Aichi, Japan) was cultured and maintained according to the manufacturer's instructions. For the high-CO₂ experiments, high-CO₂ concentration and control formulations were applied to the surface of the 3D epidermis for 12 h. Next, the cells and 3D epidermis were washed with Dulbecco's phosphate buffered saline (DPBS; Gibco) and exposed to 20 mJ/cm² UVB using a BIO-UV EXPOSURE instrument (SEN LIGHTS Co. Ltd, Osaka, Japan).

Intra-epidermal pH imaging. For intra-epidermal pH imaging, multiphoton laser microscopy (DermaInspect; JenLab, Jena, Germany) was applied. Since the fluorescence lifetime (FT) of 2',7'-bis(carboxyethyl)-4 or 5-carboxyfluorescein (BCECF) has been shown to correlate with pH⁵⁴, the FT was used as an indicator of intra-epidermal pH. The culture medium of the 3D epidermis was replaced with Hanks' balanced salt solution (HBSS; Gibco) supplemented with BCECF or BCECF-AM (DOJINDO, Kumamoto, Japan) at a final concentration of 10 μM. After 15 min, the 3D epidermis was washed with HBSS solution and used for pH imaging, whereby 3–5 mW of laser light was focused on to the epidermis from 10 μm above the insert membrane. Fluorescent images were acquired inside the epidermis and analyzed using SPC Image 2.9.4 (Becker & Hickl GmbH, Berlin, Germany). A bi-exponential fit was used on the fluorescence decay profiles, and the FT was determined for each pixel, with the largest value recorded as the representative FT of the image.

G protein-coupled receptor (GPCR) expression measurement. To measure GPCR expression, HEK293T were grown to 50% confluence and collected for RNA extraction. Digital PCR was performed on a QuantStudio 3D Digital PCR System platform consisting of a ProFlex PCR machine (including a chip adapter kit), an automatic chip loader, and a QuantStudio 3D Instrument (Life Technologies, Carlsbad, CA, USA). Specific TaqMan probes for digital PCR (Supplementary Table 1; see Supplementary Information) were selected from the TaqMan Gene Expression Assay (Applied Biosystems, Foster City, CA, USA).

siRNA experiments. HEK293T were grown to 50% confluence and transfected with specific siRNA against GPR65 or control non-target siRNA (Dharmacon, Lafayette, CO, USA) using Lipofectamine RNAiMAX transfection reagent (Invitrogen, Carlsbad, CA, USA) according to the manufacturer's instructions. After 48 h, the cells were used for the high-CO₂ experiments.

cAMP measurement. HEK293T transfected with siRNA for 48 h were incubated under 15% CO₂ for 24 h in the presence of the phosphodiesterase inhibitor 0.5 mM 3-isobutyl-1-methylxanthine (Sigma-Aldrich, St. Louis, MO, USA) and then collected. Intracellular cAMP concentration was measured using a cAMP-Glo Assay (Promega, Madison, WI, USA) according to the manufacturer's instructions.

RNA isolation and qRT-PCR. HEK293T and the 3D epidermis were collected 8 h after UVB exposure. Total RNA was isolated using an RNeasy Mini Kit (Qiagen, Hilden, Germany) reverse-transcribed into cDNA using a High Capacity RNA-to-cDNA Kit (Applied Biosystems). Quantitative real-time PCR (qRT-PCR) was performed

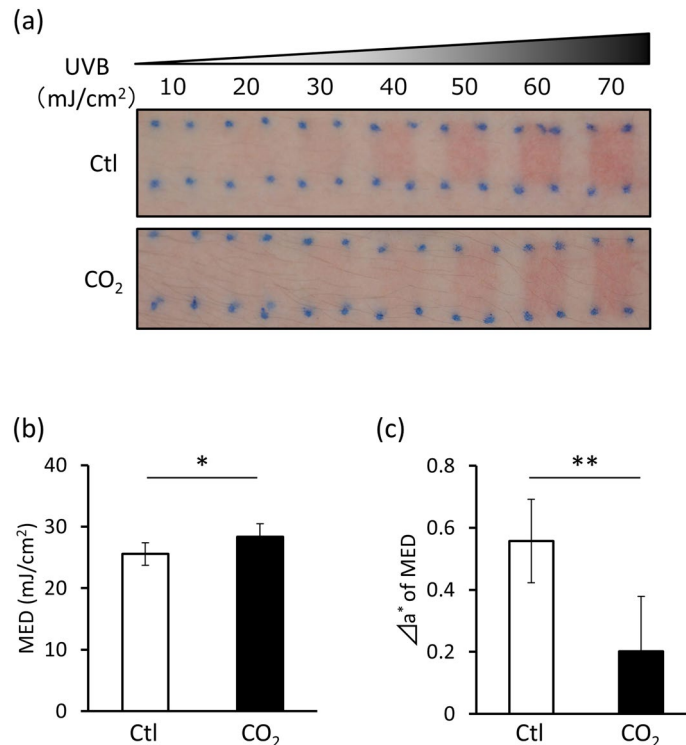


Figure 4. CO₂ inhibits UVB-induced erythema in human skin. CO₂-free (Ctl) and high-CO₂ concentration (CO₂) formulations were applied to the skin of the inner upper left arm twice daily for 2 weeks and then exposed to UVB. The next day, (a) UVB-irradiated skin images were obtained. The images shown are representative of the nine volunteers. (b) MED and (c) color-difference (Δa^* of MED) were assessed ($n=9$, $*P<0.05$, $**P<0.01$, paired Student's *t* test).

using a TaqMan Gene Expression Assay (Applied Biosystems) with specific probes for each target gene (Supplementary Table 2; see Supplementary Information). Results were normalized to RPLP0.

Enzyme-linked immunosorbent assay (ELISA). TNF α and IL-6 concentrations in the culture media of HEK_n were measured using cytokine ELISA kits (Diaclone, Besancon, France) according to the manufacturer's instructions. Absorbance was measured using an SH-9000 Lab microplate reader (Corona Electric, Ibaragi, Japan).

Western blotting. For whole-cell protein extraction, HEK_n were treated with radio-immunoprecipitation assay (RIPA) lysis buffer (Thermo Fisher Scientific, San Jose, CA, USA) supplemented with a protease/phosphatase inhibitor cocktail (Cell Signaling Technology, Beverly, MA, USA). For nuclear and cytoplasmic extraction, a nuclear extraction kit (Active Motif, Carlsbad, CA, USA) was used according to the manufacturer's instructions. Protein was quantified in each lysate using a BCA protein assay kit (Thermo Fisher Scientific), and lysates containing equal amounts of proteins were loaded onto Mini-PROTEAN TGX gels (Bio-Rad, Hercules, CA, USA), electrophoresed, and transferred to 0.2- μ m polyvinylidene fluoride (PVDF) membranes using a Trans-Blot Turbo System (Bio-Rad). The membranes were blocked with PVDF Blocking Reagent (TOYOBO, Osaka, Japan) and incubated with primary and horseradish peroxidase (HRP)-conjugated secondary antibodies (Supplementary Table 3; see Supplementary Information). Bound antibodies were detected using ECL Prime Western Blotting Detection Reagent (GE Healthcare, Arlington Heights, IL, USA).

Human study. The present study was approved by the Ethical Committee of Kao Corporation and conducted in accordance with the study protocol, ethical guidelines for clinical research, and ethical principles based on the Helsinki Declaration; it was registered with the UMIN Clinical Trials Registration System and is publicly available (# UMIN000019152). All study participants were informed regarding the content matter of the present study, and they provided informed consent. A total of nine healthy Japanese men between 20 and 50 years were recruited for this double-blind, placebo-controlled study. High-CO₂ and control formulations were applied to a designated area (5 \times 15 cm) on the inside of the left upper arm twice daily (morning and night). After 2 weeks, each site was irradiated with 10, 20, 30, 40, 50, 60, or 70 mJ/cm² of UVB (light source: UV-B lamp, GL20SE; Sankyo Denki, Kanagawa, Japan). The following day, minimal erythema dose (MED) was judged, and color was measured using a spectrophotometer to confirm erythema formation. The a^* value of the L $^*a^*b^*$ colorimetric system was used as an index of erythema.

Statistical analysis. Data are presented as the mean \pm SEM. For the experiments using HEK293 and 3D epidermis, between-group differences were analyzed by the unpaired Student's *t* tests, Dunnett's test, or Tukey–Kramer multiple comparison tests, as appropriate. For the human study, between-group differences were analyzed by the paired Student's *t* tests.

Data availability

The datasets generated during and/or analyzed during the current study are available from the corresponding author on reasonable request.

Received: 17 July 2020; Accepted: 1 December 2020

Published online: 11 January 2021

References

- Rawlings, A. V. & Harding, C. R. Moisturization and skin barrier function. *Dermatol. Ther.* **17**(Suppl 1), 43–48 (2004).
- Barker, J. N., Mitra, R. S., Griffiths, C. E., Dixit, V. M. & Nickoloff, B. J. Keratinocytes as initiators of inflammation. *Lancet* **337**, 211–214 (1991).
- Slominski, A. T., Zmijewski, M. A., Plonka, P. M., Szaflarski, J. P. & Paus, R. How UV light touches the brain and endocrine system through skin, and why. *Endocrinology* **159**, 1992–2007 (2018).
- Kim, Y. & He, Y. Y. Ultraviolet radiation-induced non-melanoma skin cancer: Regulation of DNA damage repair and inflammation. *Genes Dis.* **1**, 188–198 (2014).
- Paz, M. L., González Maglio, D. H., Weill, F. S., Bustamante, J. & Leoni, J. Mitochondrial dysfunction and cellular stress progression after ultraviolet B irradiation in human keratinocytes. *Photodermatol. Photoimmunol. Photomed.* **24**, 115–122 (2008).
- Kleszczyński, K. *et al.* Melatonin and its metabolites ameliorate UVR-induced mitochondrial oxidative stress in human MNT-1 melanoma cells. *Int. J. Mol. Sci.* **19**, 3786 (2018).
- Marais, T. L. D. *et al.* Transcription factors and stress response gene alterations in human keratinocytes following solar simulated ultra violet radiation. *Sci. Rep.* **7**, 13622 (2017).
- Gęgotek, A. & Skrzydlewska, E. The role of transcription factor Nrf2 in skin cells metabolism. *Arch. Dermatol. Res.* **307**, 385–396 (2015).
- Janjetovic, Z. *et al.* Melatonin and its metabolites protect human melanocytes against UVB-induced damage: Involvement of NRF2-mediated pathways. *Sci. Rep.* **7**, 1274 (2017).
- Griffiths, C. E. M., van de Kerkhof, P. & Czarnecka-Operacz, M. Psoriasis and atopic dermatitis. *Dermatol. Ther. (Heidelb)*. **7**(Suppl 1), 31–41 (2017).
- Cummins, E. P., Selfridge, A. C., Sporn, P. H., Sznajder, J. I. & Taylor, C. T. Carbon dioxide-sensing in organisms and its implications for human disease. *Cell. Mol. Life Sci.* **71**, 831–845 (2014).
- Chandrashekar, J. *et al.* The taste of carbonation. *Science* **326**, 443–445 (2009).
- Frommer, W. B. CO₂ mmon sense. *Science* **327**, 275–276 (2010).
- Papapetropoulos, A., Foresti, R. & Ferdinandy, P. Pharmacology of the “gasotransmitters” NO, CO and H₂S: Translational opportunities. *Br. J. Pharmacol.* **172**, 1395–1396 (2015).
- Cals-Grierson, M. M. & Ormerod, A. D. Nitric oxide function in the skin. *Nitric Oxide* **10**, 179–193 (2004).
- Coavoy-Sánchez, S. A., Costa, S. K. P. & Muscará, M. N. Hydrogen sulfide and dermatological diseases. *Br. J. Pharmacol.* **177**, 857–865 (2020).
- Amato, M. B. *et al.* Effect of a protective-ventilation strategy on mortality in the acute respiratory distress syndrome. *N. Engl. J. Med.* **338**, 347–354 (1998).
- Laffey, J. G. *et al.* Hypercapnic acidosis attenuates endotoxin-induced acute lung injury. *Am. J. Respir. Crit. Care Med.* **169**, 46–56 (2004).
- Costello, J. *et al.* Hypercapnic acidosis attenuates shock and lung injury in early and prolonged systemic sepsis. *Crit. Care Med.* **37**, 2412–2420 (2009).
- Takeshita, K. *et al.* Hypercapnic acidosis attenuates endotoxin-induced nuclear factor- κ B activation. *Am. J. Respir. Cell Mol. Biol.* **29**, 124–132 (2003).
- O’Toole, D. *et al.* Hypercapnic acidosis attenuates pulmonary epithelial wound repair by an NF- κ B dependent mechanism. *Thorax* **64**, 976–982 (2009).
- Wang, N. *et al.* Elevated CO₂ selectively inhibits interleukin-6 and tumor necrosis factor expression and decreases phagocytosis in the macrophage. *FASEB J.* **24**, 2178–2190 (2010).
- Brandi, C. *et al.* The role of carbon dioxide therapy in the treatment of chronic wounds. *In Vivo* **24**, 223–226 (2010).
- Penhavel, M. V. C., Nascimento, V. H. T., Durães, E. F. R., Carneiro, F. P. & de Sousa, J. B. Effects of carbon dioxide therapy on the healing of acute skin wounds induced on the back of rats. *Acta Cir. Bras.* **28**, 334–339 (2013).
- Yuki, K., Kawano, S., Mori, S. & Murase, T. Facial application of high-concentration carbon dioxide prevents epidermal impairment associated with environmental changes. *Clin. Cosmet. Investig. Dermatol.* **12**, 63–69 (2019).
- Sindrilaru, A. *et al.* An unrestrained proinflammatory M1 macrophage population induced by iron impairs wound healing in humans and mice. *J. Clin. Investig.* **121**, 985–997 (2011).
- Hänel, K. H., Cornelissen, C., Lüscher, B. & Baron, J. M. Cytokines and the skin barrier. *Int. J. Mol. Sci.* **14**, 6720–6745 (2013).
- Okajima, F. Regulation of inflammation by extracellular acidification and proton-sensing GPCRs. *Cell Signal.* **25**, 2263–2271 (2013).
- Geiger, T. *et al.* Induction of rat acute-phase proteins by interleukin 6 in vivo. *Eur. J. Immunol.* **18**, 717–721 (1988).
- Kondo, S. & Sauder, D. N. Tumor necrosis factor (TNF) receptor type 1 (p55) is a main mediator for TNF- α -induced skin inflammation. *Eur. J. Immunol.* **27**, 1713–1718 (1997).
- Ito, T., Moore, J. I. & Koss, M. C. Topical application of CO₂ increases skin blood flow. *J. Investig. Dermatol.* **93**, 259–262 (1989).
- Duling, B. R. Changes in microvascular diameter and oxygen tension induced by carbon dioxide. *Circ. Res.* **32**, 370–376 (1973).
- Kleszczyński, K., Tukaj, S., Kruse, N., Zillikens, D. & Fischer, T. W. Melatonin prevents ultraviolet radiation-induced alterations in plasma membrane potential and intracellular pH in human keratinocytes. *J. Pineal Res.* **54**, 89–99 (2013).
- Proksch, E. pH in nature, humans and skin. *J. Dermatol.* **45**, 1044–1052 (2018).
- Jang, H. *et al.* Skin pH is the master switch of kallikrein 5-mediated skin barrier destruction in a murine atopic dermatitis model. *J. Investig. Dermatol.* **136**, 127–135 (2016).
- Lee, H. J. *et al.* Acidification of stratum corneum prevents the progression from atopic dermatitis to respiratory allergy. *Exp. Dermatol.* **26**, 66–72 (2017).
- Lee, N. R. *et al.* Application of topical acids improves atopic dermatitis in murine model by enhancement of skin barrier functions regardless of the origin of acids. *Ann. Dermatol.* **28**, 690–696 (2016).
- Wemmie, J. A., Price, M. P. & Welsh, M. J. Acid-sensing ion channels: Advances, questions and therapeutic opportunities. *Trends Neurosci.* **29**, 578–586 (2006).

39. Behne, M. J. *et al.* NHE1 regulates the stratum corneum permeability barrier homeostasis. Microenvironment acidification assessed with fluorescence lifetime imaging. *J. Biol. Chem.* **277**, 47399–47406 (2002).
40. Hachem, J. P. *et al.* Extracellular pH controls NHE1 expression in epidermis and keratinocytes: Implications for barrier repair. *J. Investig. Dermatol.* **125**, 790–797 (2005).
41. Im, D. S., Heise, C. E., Nguyen, T., O'Dowd, B. F. & Lynch, K. R. Identification of a molecular target of psychosine and its role in globose cell formation. *J. Cell Biol.* **153**, 429–434 (2001).
42. Wang, J. Q. *et al.* TDAG8 is a proton-sensing and psychosine-sensitive G-protein-coupled receptor. *J. Biol. Chem.* **279**, 45626–45633 (2004).
43. Ishii, S., Kihara, Y. & Shimizu, T. Identification of T cell death-associated gene 8 (TDAG8) as a novel acid sensing G-protein-coupled receptor. *J. Biol. Chem.* **280**, 9083–9087 (2005).
44. Radu, C. G., Nijagal, A., McLaughlin, J., Wang, L. & Witte, O. L. Differential proton sensitivity of related G protein-coupled receptors T cell death-associated gene 8 and G2A expressed in immune cells. *Proc. Natl. Acad. Sci. U.S.A.* **102**, 1632–1637 (2005).
45. Dorsam, R. T. & Gutkind, J. S. G-protein-coupled receptors and cancer. *Nat. Rev. Cancer* **7**, 79–94 (2007).
46. Assefa, Z., Van Laethem, A., Garmyn, M. & Agostinis, P. Ultraviolet radiation-induced apoptosis in keratinocytes: On the role of cytosolic factors. *Biochim. Biophys. Acta* **1755**, 90–106 (2005).
47. Cummins, E. P. *et al.* NF- κ B links CO₂ sensing to innate immunity and inflammation in mammalian cells. *J. Immunol.* **185**, 4439–4445 (2010).
48. Tsuchiya, Y. *et al.* Nuclear IKK β is an adaptor protein for IkappaB α ubiquitination and degradation in UV-induced NF-kappaB activation. *Mol. Cell* **39**, 570–582 (2010).
49. Pasparkis, M., Haase, I. & Nestle, F. O. Mechanisms regulating skin immunity and inflammation. *Nat. Rev. Immunol.* **14**, 289–301 (2014).
50. Schafer, P. H. *et al.* Apremilast, a cAMP phosphodiesterase-4 inhibitor, demonstrates anti-inflammatory activity in vitro and in a model of psoriasis. *Br. J. Pharmacol.* **159**, 842–855 (2010).
51. Andoh, T., Yoshida, T. & Kuraishi, Y. Topical E6005, a novel phosphodiesterase 4 inhibitor, attenuates spontaneous itch-related responses in mice with chronic atopy-like dermatitis. *Exp. Dermatol.* **23**, 359–361 (2014).
52. Keating, G. M. Apremilast: A review in psoriasis and psoriatic arthritis. *Drugs* **77**, 459–472 (2017).
53. Hoy, S. M. Crisaborole ointment 2%: A review in mild to moderate atopic dermatitis. *Am. J. Clin. Dermatol.* **18**, 837–843 (2017).
54. Hanson, K. M. *et al.* Two-photon fluorescence lifetime imaging of the skin stratum corneum pH gradient. *Biophys. J.* **83**, 1682–1690 (2002).

Acknowledgements

We would like to thank Chiaki Sone and Masaru Hosokawa for providing the test samples at Skin Care Laboratories, Kao Corporation. We would also like to thank Editage for editing and reviewing this manuscript for the English language.

Author contributions

Conceptualization: K.S.A. and T.Y.; Data curation: K.S.A., K.Y., and K.S.U.; Formal analysis: K.S.A., K.Y., and K.S.U.; Investigation: K.S.A., K.Y., K.S.U., and S.F.; Methodology: K.S.A., K.Y., and K.S.U.; Project administration: T.M. and T.Y.; Resources: T.M.; Supervision: T.M.; Validation: K.S.A.; Visualization: K.S.A.; Writing original draft: K.S.A.; Writing review and editing: T.M. and S.I. All authors read and approved the final manuscript.

Competing interests

The authors declare no competing interests.

Additional information

Supplementary Information The online version contains supplementary material available at <https://doi.org/10.1038/s41598-020-79519-0>.

Correspondence and requests for materials should be addressed to T.M.

Reprints and permissions information is available at www.nature.com/reprints.

Publisher's note Springer Nature remains neutral with regard to jurisdictional claims in published maps and institutional affiliations.



Open Access This article is licensed under a Creative Commons Attribution 4.0 International License, which permits use, sharing, adaptation, distribution and reproduction in any medium or format, as long as you give appropriate credit to the original author(s) and the source, provide a link to the Creative Commons licence, and indicate if changes were made. The images or other third party material in this article are included in the article's Creative Commons licence, unless indicated otherwise in a credit line to the material. If material is not included in the article's Creative Commons licence and your intended use is not permitted by statutory regulation or exceeds the permitted use, you will need to obtain permission directly from the copyright holder. To view a copy of this licence, visit <http://creativecommons.org/licenses/by/4.0/>.

© The Author(s) 2021